City Research Online

City, University of London Institutional Repository

Plastic fiber design for THz generation through wavelength translation

Ajanta Barh,[1,*] R. K. Varshney,[1] G. P. Agrawal,[2] B. M. A. Rahman,[3] and B. P. Pal[4]

[1]*Physics Department, Indian Institute of Technology Delhi, Hauz Khas, New Delhi 110016, India*
[2]*Institute of Optics, University of Rochester, Rochester, NY 14627, USA*
[3]*Department of Electrical and Electronic Engineering, City University London, London EC1V 0HB, U.K.*
[4]*School of Natural Sciences, Mahindra Ecole Centrale, Hyderabad 500043, India*
Corresponding author: ajanta.barh@gmail.com

We report on an all-fiber Terahertz (THz) radiation source by exploiting nonlinear parametric process in a theoretically designed microstructured-core double clad plastic fiber (MC-DCPF). The required phase-matching condition is satisfied through suitable tailoring of the fiber dispersion and nonlinear properties at the pump wavelength of a high power CO_2 laser, with a CO laser of much lower power acting as a seed concomitantly. Our simulated results reveal that a THz radiation source at the frequency of ~ 3 THz could be realized with a 3-dB phase-matching band-width of 2.13 GHz in a 65 m long optimized MC-DCPF. Maximum power conversion efficiency >1% is realizable even after including the material loss.

The frequency of Terahertz (THz) radiation or T-rays extends from 0.1 to 10 THz (3 mm to 30 μm), a range that bridges the gap (sometimes known as the THz gap) between microwaves and infrared light [1]. In early days T-rays were used only for *passive* applications, where THz radiation was detected to analyze the astronomical objects and to study the chemistry of outer space. However over the last 15 years, THz based *active* applications have emerged which require a high power THz source, an efficient detection technique, and transmission of THz via wave-guiding. In one hand, the vibrational/rotational transitions of a wide range of molecular clusters and the electronic transitions of various nano-composites exhibit strong resonances at THz frequencies [2]. On the other hand, such T-rays penetrate deep inside many materials, such as cloths, papers, wood, ceramics, polymers, walls, dry air etc. These features make THz extremely useful for spectroscopy, sensing, imaging, tomography, medical diagnostics, study of protein dynamics, spintronics, astronomy etc. [1-6]. Moreover, T-rays do not pass through metals, dust and water, making them popular for security and defense applications [6]. THz waves are also employed for short-distance wireless communication [7].

All these aforementioned applications require efficient tunable, broad-band THz sources. Several schemes have already been proposed for generating THz waves. Because of the high frequencies involved, THz generation and detection is quite challenging in conventional electronic devices, which generally operate below 100 GHz. T-rays suffer from high metallic losses, and suitable electro-optic devices are also not available. Optical techniques-based THz generation is limited by the lack of suitable narrow band-gap semiconductor materials. As an alternative, two schemes for THz generation have been employed: one is based on accelerating charge particle [8] and the other is based on modulation of local polarization [2]. Under the first scheme, proposals based on a free-electron laser [8] or synchrotron radiation [8,9] generate THz radiations with very high powers (kW to MW level) over a widely tunable range. However, these setups are bulky and quite expensive for regular use. Under the second scheme, laser-induced nonlinear effects have been exploited to generate THz wave either by initiating resonant or non-resonant processes. In recent years, several approaches have been proposed, based on e.g. PC antenna [10] or dipole antenna [2], optical rectification [11], difference frequency generation in nonlinear crystals [2,12], polymer materials [13], quantum cascade laser [14] etc. In most of these cases, the output THz power is typically very low (μW – mW level) though broad-band output with a compact design is possible. Other approaches include surface emission in a magnetic field [2] and magnetic component of light induced charge separation in dielectric [15]. However, the power conversion efficiency remains extremely poor (10^{-4} - 10^{-6}) in all cases.

Since optical fiber-based applications are attractive for day-to-day life (medical endoscopy, diagnostics, sensing, communication etc.), there exists a strong interest for THz generation via optical fibers. Some advances have been already made in this direction, e.g., nonlinear parametric amplification with surface emission [16]. Though tunable THz output is realizable by this approach, the efficiency is still quite low (~10^{-6}). In this paper, we analyze theoretically *fiber*-based efficient generation of THz radiation by exploring degenerate-four wave mixing (D-FWM). One sure way to increase its efficiency is to improve the modal overlap among participating waves. In order to achieve this, we propose a microstructured-core double-clad plastic fiber (MC-DCPF). Low-loss plastic, Teflon is taken to be the fiber base material [17] and commercially available high power CO_2 and CO lasers emitting near 10.6 μm and 5.59 μm are employed as

pump and seed for the D-FWM process, respectively. Through our simulations, we show that, for a continuous wave (CW) pump of 1 kW power and input idler of ~ 20 W power, CW THz output near 3 THz is achievable in a 65 m long optimized MC-DCPF with a conversion efficiency (η) of more than two orders of magnitude ($\eta > 10^{-2}$) higher than what have been reported to date.

Although several nonlinear processes can be exploited to generate new frequencies [18], FWM is the most relevant process for THz generation, provided the required phase matching condition can be satisfied. In the D-FWM process, two pump photons of the same frequency (ω_p) are converted to a signal photon ($\omega_s < \omega_p$) and an idler photon ($\omega_i > \omega_p$), satisfying the energy conservation relation ($2\omega_p = \omega_s + \omega_i$); the subscripts p, s and i stand for pump, signal and idler, respectively. The frequency shift ($\Omega_s = \omega_p - \omega_s$) strongly depends on the group velocity dispersion (GVD) and nonlinear parameters of the fiber at the pump wavelength (λ_p), which should ideally lie close to the designed fiber's zero dispersion wavelength. The FWM efficiency strongly depends on the residual phase mismatch, modal overlap among three waves, effective nonlinearity of the fiber, and fiber's losses [19]. Assuming CW conditions for all the three waves, their evolution in the fiber in terms of their complex amplitudes, $A_j(z)$ (where, j = p, s, i) is governed by the following three coupled equations [19]:

$$\frac{dA_p}{dz} = -\frac{\alpha_p A_p}{2} + \frac{in_2\omega_p}{c}\left[\begin{array}{c}\left(f_{pp}|A_p|^2 + 2\sum_{k=i,s} f_{pk}|A_k|^2\right)A_p \\ + 2f_{ppis}A_p^* A_i A_s e^{j\Delta k_L z}\end{array}\right] \quad (1)$$

$$\frac{dA_i}{dz} = -\frac{\alpha_i A_i}{2} + \frac{in_2\omega_i}{c}\left[\begin{array}{c}\left(f_{ii}|A_i|^2 + 2\sum_{k=p,s} f_{ik}|A_k|^2\right)A_i \\ + f_{ispp}A_s^* A_p^2 e^{-j\Delta k_L z}\end{array}\right] \quad (2)$$

$$\frac{dA_s}{dz} = -\frac{\alpha_s A_s}{2} + \frac{in_2\omega_s}{c}\left[\begin{array}{c}\left(f_{ss}|A_s|^2 + 2\sum_{k=p,i} f_{sk}|A_k|^2\right)A_s \\ + f_{sipp}A_i^* A_p^2 e^{-j\Delta k_L z}\end{array}\right] \quad (3)$$

These equations include pump depletion, losses in the fiber (α_j), and all the necessary Kerr terms. The f_{ij} and f_{ijkl} are overlap parameters [18], Δk_L is the linear phase mismatch term (contribution from GVD), which is compensated by self-phase or cross-phase modulation to satisfy the phase matching condition. Considering up to 5th order GVD, the Ω_s could be approximated as [19]

$$\Omega_s = \sqrt{\frac{6|\beta_2|}{\beta_4}\left(1 \pm \sqrt{1 - \frac{\beta_4\gamma P_0}{3\beta_2^2}}\right)} \quad (4)$$

where, β_m is the mth order GVD parameter, γ is the NL parameter and P_0 is the input pump power. For our design task, *multi-order* dispersion management is extremely crucial. Our design target has been to achieve flat dispersion with suitably small values of β_2 and β_4 of opposite signs around λ_p. The parameter n_2 appearing in Eqs. (1) – (3) is expected to vary with the wavelength [18]. In this study we have assumed its value to be same at the

three participating waves. From the literature review it is evident that several polymer materials exhibit high optical Kerr nonlinearity when prepared with proper processing and doping ($n_2 \sim 10^{-18} - 10^{-17}$ m²/W) [20]. According to Ref. [21], an aqueous suspension of Teflon micro-ellipsoids can acquire exceedingly high value of $n_2 \sim 10^{-14}$ m²/W, though it may be lower for bulk Teflon. As no universal data for n_2 of bulk Teflon is available in literature till date, we have assumed a nominal value of $n_2 \sim 10^{-17}$ m²/W (similar to other polymers) for Teflon fiber throughout our numerical analysis.

Our primary aim is to improve the modal overlap among the input optical (pump and idler) and generated THz waves, along with a proper dispersion profile at λ_p in order to achieve efficient generation of THz waves. However, the fiber should be effectively single-moded with a low loss. Since wavelengths of different waves involved in the parametric process are very different, it is a challenge to satisfy all the aforementioned criteria simultaneously. We balanced them by choosing optimal fiber parameters of our proposed double clad fiber design. For the fiber structure, we consider three kinds of Teflon materials with slightly different refractive indices. These are easily available in the market as different commercial suppliers can provide Teflon with different refractive indices [17]. As a first step in design recipe, we considered a microstructured-core (MC) based *large mode area* fiber (similar to that used in [22]) to realize an ultra-high effective mode area (A_{eff}) at λ_p and λ_i; a schematic cross-sectional view of the MC fiber is shown in Fig. 1(a). The MC is formed by using 4 rings of hexagonally arranged higher index rods ($n_r = 1.44$, Teflon-type-1 shown as white circles in Fig. 1(a)) embedded in a lower index background ($n_b \sim 1.425$, Teflon-type-2, dark blue in color), which also forms the uniform cladding (1st cladding) for λ_p and λ_i. The radius of high index rods and pitch in the MC are denoted by r and Λ, respectively, which were optimized to 1 µm and 30 µm, respectively for achieving effective single-mode operation with low confinement loss (α_c) over the concerned spectral range. Though the MC fiber is multimoded, the value of α_c for higher-order modes is more than 5 orders of magnitudes higher, and hence these leak away rapidly within a short length of propagation.

For THz wave ($\lambda_s \sim 100$ µm), this structure, as a whole, (Fig. 1(a)) acts as the fiber core with refractive index equivalent to the average index of that region (n_{av}, light purple color in Fig. 1(b)). Now by adding another cladding (2nd clad of refractive index, $n_{cl} = 1.4$, Teflon-type-3, light blue color in Fig. 1(b)) around this equivalent core, we can define an equivalent step-index fiber (E-SIF) structure for THz wave (cf. Fig. 1(b)). For this E-SIF structure, the core radius (R_1) is optimized to 150 µm by limiting the fiber V number to near about 2.4 [23], so that single-mode operation can be established for THz also. The outer boundary of this cladding (radius R_2) is fixed to get negligible α_c at the THz wavelength. Combining these two structures, we propose a MC-DCPF geometry (cf. Fig. 1(c)), where modal overlap between the three waves can be up to ~ 70%. The GVD parameters as well as the modal fields were calculated with the open access CUDOS software, and Eqs. (1) to (3) were solved in MATLAB®.
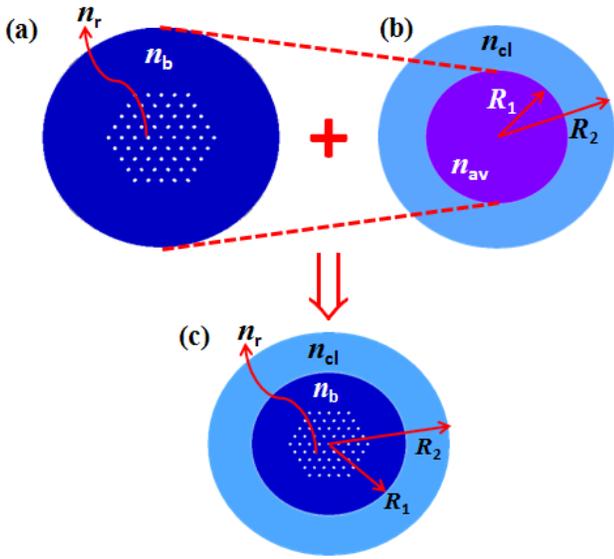
Fig. 1. (a) Effective cross-section of the designed fiber for optical waves. The core is formed by hexagonally arranged 4 rings of high index rods of radius = 1 μm (white circles) and of pitch = 30 μm in a uniform lower index background of much wider cross-section (dark blue color), which effectively forms the cladding; (b) Effective cross-section for the THz wave, where core of radius R_1 is formed by an average index (n_{av}, light purple color) with uniform cladding (2nd clad, shown in light blue color); (c) The combined cross-section of the proposed MC-DCPF.

We have assumed the commercially available high power CO_2 laser to be the input pump ($\lambda_p \sim 10.6$ μm). In order to realize THz output at ~ 3 THz ($\lambda_s \sim 100$ μm), the required λ_i becomes ~ 5.59 μm, which is coincidently close to the wavelength of commercially available CO lasers. It is important to mention that, launching of a weak idler along with the pump improves the FWM efficiency considerably as it stimulates the FWM process. We have studied the modal properties of the three waves and investigated their dispersion behavior around λ_p in order to find the GVD parameters. Since the effective contribution (in terms of weighted percentage) of the region with index n_b is much larger than the other regions (indices n_r and n_{cl}), we have employed a proper material dispersion model for n_b but used fixed values for n_r and n_{cl}. The variation of β_2 and β_4 with wavelength for the optimum fiber structure is shown in Figs. 2(a) and 2(b), respectively. The optimum values of β_2 and β_4 are found to be -8.94 ps²/km and 4.23×10^{-3} ps⁴/km, respectively at λ_p = 10.58 μm. For an input pump power (P_0) of 1 kW, the THz wave is generated centered at 99.45 μm (≈ 3.0145 THz).

We have also studied the evolution of three waves with propagation by numerically solving Eqs. (1) – (3). We define the amplification factor (AF) as the ratio of output and input power, such that, $AF_j = P_{j,out}/P_{i,in}$ for j = i, s and $P_{j,out}/P_0$ for j = p, where, $P_{j,out}$ is the output power and $P_{i,in}$ is the input idler power. Changes in AF for these three waves along fiber length (L) are plotted in Fig. 3(a) for a $P_{i,in}$ = 20 W. Power variations are plotted in Fig. 3(b). Both figures reveal that the maximum power transfer from pump to generated THz wave takes place at L = 64.7 m. It is worthwhile to mention that, for the proposed MC-DCPF, A_{eff} at the pump and generated THz waves are

extremely large (~ 36,000 μm² and 78,000 μm², respectively). As a result, though we have assumed a relatively high power at the input, the effective intensity was only ~ 0.003 GW/cm², which is much lower than the potential onset of other resonance based nonlinear effects.
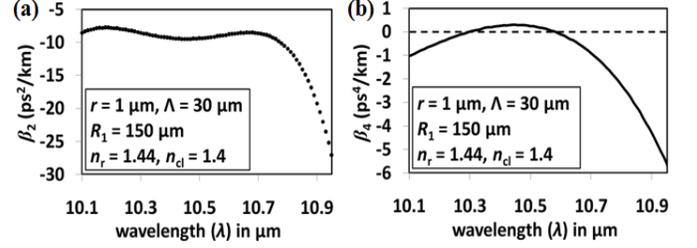

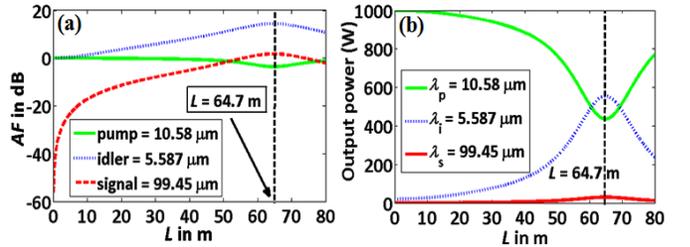Fig. 2. Variation of (a) β_2 and (b) β_4 with the operating wavelength around pump for optimum fiber parameters.

Fig. 3. Variation of (a) AF and (b) output power along fiber length (L) for λ_P = 10.58 μm (green color), λ_s = 99.45 μm (red color) and λ_i = 5.587 μm (blue color).

Even after including pump depletion, THz power of > 30 W is achievable (cf. Fig. 3(b)) with a power conversion efficiency, η ($=P_{s,out}/P_0$) $> 3 \times 10^{-2}$, which, to our knowledge, is the best result till date. We have also investigated the effect of *seeding* on the AF and found that, it essentially dictates the optimum fiber length (L_{opt}). The variation of L_{opt} with $P_{i,in}$ is plotted in Fig. 4(a), where we see an inverse relationship between the two. We may mention that L_{opt} can be further reduced by increasing the effective nonlinearity [$\gamma = (2\pi n_2)/(\lambda A_{eff})$] of the medium. The *phase-matching band-width* (BW) of the generated THz signal is investigated by studying the variations of $P_{s,out}$ around the generated T-ray (3.015 THz) (shown in Fig. 4(b)), where the 3-dB BW is ~ 2.13 GHz (≈ 70 nm). Further by tuning the λ_p, generated λ_s can be tuned.
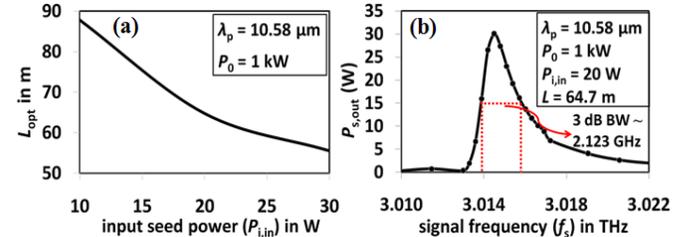

Fig. 4. (a) Variation of optimum fiber length with input seed idler power for a fixed pump power of 1 kW. (b) Output spectrum of generated THz wave; 3-dB phase-matching band-width is ~ 2.13 GHz (≈ 70 nm).

Variation of the pointing vector (S_z) along the x direction is plotted for both the pump and THz-wave as shown in Fig. 5(a). This shows the confinement of lower THz frequency is lower, as expected, however, we have been able to make the them reasonably similar. The preceding results neglected fiber losses. We briefly discuss

the impact of material loss of Teflon. According to the commercial datasheet [17], Teflon with quite good transmission at all the three wavelengths of interest can be fabricated. After inclusion of the loss (0.01 m⁻¹), η becomes 0.01. Although smaller by a factor 3 compared to the loss-free case, it is still 2 orders of magnitude higher than the previously reported results in the literature.

The length of our proposed fiber is relatively long. To make a compact device, fiber can be wrapped around a circular mandrel/bobbin. However this may lead to intolerable bend-loss (α_b). Keeping this in mind, we have studied α_b of the proposed MC-DCPF at THz wavelength by considering E-SIF approximation and using the following formula for pure bend-loss [23]:

$$\alpha_b = \frac{1}{8}\sqrt{\frac{\pi}{R_1 R_b W^3}} S(V,W)\exp\left[-\frac{4R_b W^3 \Delta}{3V^2 R_1}\right] \qquad (5)$$

where, $S(V,W) = \frac{R_1^2}{K_0^2(W)}\left[\int_0^\infty \frac{E^2(r)}{E^2(R_1)} r\,dr\right]^{-1} \qquad (6)$

R_1 is the core radius, R_b is the bend radius, V, W and Δ are the conventional fiber parameters as described in [23] and the function $S(V,W)$ can be calculated from modal field distribution $E(r)$ and K_0 is the zero$^{\text{th}}$ order modified Bessel function. The variation of α_b with R_b for the proposed MC-DCPF is plotted in Fig. 5(b). Estimated bend-loss can be seen to be quite low for the proposed fiber structure. More specifically, it becomes negligible for $R_b \geq$ 10 cm, which is quite favorable for our targeted design.
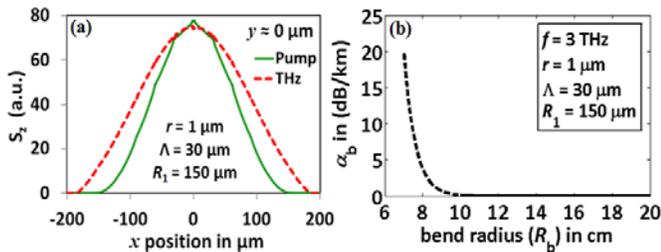

Fig. 5. (a) 1-D variation of pointing vector (S_z) for pump and THz wave. (b) Variation of bend-loss (α_b) as a function of bend radius (R_b) of the proposed MC-DCPF at ~ 3 THz.

In conclusion, we report a theoretical design of efficient fiber-based THz source by exploiting D-FWM process in a Teflon-based novel MC-DCPF. Our target was to employ commercially available high power mid-IR light sources as the pump and seed idler in order to generate THz radiation via nonlinear D-FWM process. The collinear phase matching condition is achieved by tailoring the design of the MC-DCPF with proper dispersion and nonlinearity around the pump wavelength. The efficiency of D-FWM process is improved by maximizing the modal overlaps among all the three waves; overlap > 70% is achieved for optical and THz waves. This is the most difficult but crucial step in our fiber design target. Effective single-mode operation is ensured throughout. For a pump of 1 kW power emitting at 10.58 µm, a THz wave centered at 3 THz could be generated with ~ 30 W of CW power at the output end of a 64.7 m long fiber of our design. Including pump depletion and material loss, the

optical to THz conversion efficiency ~ 1% should be realizable, which is ~ 2 orders of magnitude higher than previously reported results. The 3-dB phase-matching band-width of the generated THz wave is about 70 nm ($\equiv$ 2.13 GHz). We have also shown that the relatively long fiber length would not be an issue since such a plastic fiber can be spooled in a circular mandrel/bobbin to make it compact for convenient handling; bend-induced loss is negligible for bend-radii $\geq$ 10 cm, which is two orders of magnitude less than a typical synchrotron setup for THz generation [8]. Our proposal should serve as the initial design platform to fabricate efficient fiber-based THz sources. The microstructured geometry is relatively simple, and should be realizable in practice as it is amenable to well-matured state-of-the-art fabrication technologies [24]

References

1. X. C. Zhang, Phys. in Medicine and Biology **47**, 3667 (2002).
2. G. Kh. Kitaeva, Laser Phys. Lett. **5**, 559 (2008).
3. D. Abbott and X.-C. Zhang, Proc. IEEE **95**, 1509 (2007).
4. M. Theuer, S. S. Harsha, D. Molter, G. Torosyan, and R. Beigang, Chem. Phys. Chem. **12**, 2695 (2011).
5. S. Wang and X. C. Zhang, J. Phys. D: Appl. Phys. **37**, R1 (2004).
6. A. G. Davies, A. D. Burnett, W. Fan, E. H. Linfield, and J. E. Cunningham, Materials Today-Rev. **11**, 18 (2008).
7. H. J. Song and T. Nagatsuma, IEEE Trans. on Terahertz Sc. and Technol. **1**, 256 (2011).
8. G. P. Williams, Reports on Prog. in Phys. **69**, 301 (2006).
9. F. Wang, D. Cheever, M. Farkhondeh, W. Franklin, E. Ihloff, J. van der Laan, B. McAllister, R. Milner, C. Tschalaer, D. Wang, D. F. Wang, A. Zolfaghari, T. Zwart, G. L. Carr, B. Podobedov, and F. Sannibale, Phys. Rev. Lett. **96**, 064801 (2006).
10. E. Budiarto, J. Margolies, S. Jeong, J. Son, and J. Bokor, IEEE J. Quant. Electro. **32**, 1839 (1996).
11. S. Xu, J. Liu, G. Zheng, and J. Li, Opt. Ex. **18**, 22625 (2010).
12. Y. J. Ding, JOSA B **31**, 2696 (2014).
13. A. Rahman, J. Molecular Struc. **1006**, 59 (2011).
14. M. A. Belkin, F. Capasso, A. Belyanin, D. L. Sivco, A. Y. Cho, D. C. Oakley, C. J. Vineis, and G. W. Turner, Nat. Photon. **1**, 288 (2007).
15. W. M. Fisher and S. C. Rand, JAP **109**, 1 (2011).
16. K. Suizu and K. Kawase, Opt. Lett. **32**, 2990 (2007).
17. www.tydexoptics.com/products/thz_optics/thz_materials/
18. G. P. Agrawal, *Nonlinear Fiber Optics*, Academic, San Diego, Calif., (2007).
19. A. Barh, S. Ghosh, R. K. Varshney, and B. P. Pal, Opt. Ex. **21**, 9547 (2013).
20. T. Kaino and Y. Katayama, Polymer Eng. and Sc. **29**, 1209 (1989).
21. R. Pizzoferrato, M. Marinelli, U. Zammit, F. Scudieri, S. Martellucci, and M. Romagnoli, Opt. Comm. **68**, 231 (1988).
22. A. Barh, S. Ghosh, R. K. Varshney, and B. P. Pal, Opt. Comm. **311**, 129 (2013).
23. E.-G. Neumann, *Single-Mode Fibers Fundamentals*, Springer-Verlag, Germany, 126 (1988).
24. A. Argyros, J. Lightwave Technol. **27**, 1571 (2009).

List of References (full version)

1. X. C. Zhang, "Terahertz wave imaging: horizons and hurdles," Phys. in Medicine and Biology **47**, 3667-3677 (2002).
2. G. Kh. Kitaeva, "Terahertz generation by means of optical lasers," Laser Phys. Lett. **5**, 559–576 (2008).
3. D. Abbott and X.-C. Zhang, "Scanning the issue: T-ray imaging, sensing, and retection," Proc. IEEE **95**, 1509-1513 (2007).
4. M. Theuer, S. S. Harsha, D. Molter, G. Torosyan, and R. Beigang, "Terahertz time-domain spectroscopy of gases, liquids, and solids," Chem. Phys. Chem. **12**, 2695-2705 (2011).
5. S. Wang and X. C. Zhang, "Pulsed terahertz tomography," J. Phys. D: Appl. Phys. **37**, R1-R36 (2004).
6. A. G. Davies, A. D. Burnett, W. Fan, E. H. Linfield, and J. E. Cunningham, "Terahertz spectroscopy of explosives and drugs," Materials Today-Review, **11**(3), 18-26 (2008).
7. H. J. Song and T. Nagatsuma, "Present and future of terahertz communications," IEEE Transactions on Terahertz science and technology, **1**(1), 256-263 (2011).
8. G. P. Williams, "Filling the THz gap—high power sources and applications," Reports on Progress in Physics, **69**(2), 301 (2006).
9. F. Wang, D. Cheever, M. Farkhondeh, W. Franklin, E. Ihloff, J. van der Laan, B. McAllister, R. Milner, C. Tschalaer, D. Wang, D. F. Wang, A. Zolfaghari, T. Zwart, G. L. Carr, B. Podobedov, and F. Sannibale, "Coherent THz synchrotron radiation from a storage ring with high-frequency RF system," Phys. Rev. Lett., **96**(6), 064801(2006).
10. E. Budiarto, J. Margolies, S. Jeong, J. Son, and J. Bokor, "High-intensity terahertz pulses at 1-kHz repetition rate," IEEE J. Quant. Electro., **32**(10), 1839-1846 (1996).
11. S. Xu, J. Liu, G. Zheng, and J. Li, "Broadband terahertz generation through intracavity nonlinear optical rectification," Opt. Exp. **18**, 22625-22630 (2010).
12. Y. J. Ding, "Progress in terahertz sources based on difference-frequency generation [Invited]," JOSA B, **31**(11), 2696-2711 (2014).
13. A. Rahman, "Dendrimer based terahertz time-domain spectroscopy and applications in molecular characterization," J. Molecular Structure **1006**, 59–65 (2011).
14. M. A. Belkin, F. Capasso, A. Belyanin, D. L. Sivco, A. Y. Cho, D. C. Oakley, C. J. Vineis, and G. W. Turner, "Terahertz quantum-cascade-laser source based on intracavity difference-frequency generation," Nature Photonics, **1**(5), 288-292 (2007).
15. W. M. Fisher and S. C. Rand, "Optically-induced charge separation and terahertz emission in unbiased dielectrics," JAP **109**, 1-8 (2011).
16. K. Suizu and K. Kawase, "Terahertz-wave generation in a conventional optical fiber," Opt. Lett., **32**(20), 2990-2992 (2007).
17. www.tydexoptics.com/products/thz_optics/thz_materials/
18. G. P. Agrawal, *Nonlinear Fiber Optics*, Academic, San Diego, Calif., (2007).
19. A. Barh, S. Ghosh, R. K. Varshney, and B. P. Pal, "An efficient broad-band mid-wave IR fiber optic light source: Design and performance simulation," Opt. Exp. **21**, 9547-9555 (2013).
20. T. Kaino and Y. Katayama, "Polymers for optoelectronics," Polymer Eng. and Sc. **29**, 1209-1214 (1989).
21. R. Pizzoferrato, M. Marinelli, U. Zammit, F. Scudieri, S. Martellucci, and M. Romagnoli, "Optically induced reorientational birefringence in an artificial anisotropic Kerr medium," Opt. Comm. **68**, 231-234 (1988).
22. A. Barh, S. Ghosh, R. K. Varshney, and B. P. Pal, "Ultra-large mode area microstructured core chalcogenide fiber design for mid-IR beam delivery," Opt. Comm. **311**, 129-133 (2013).
23. E.-G. Neumann, *Single-Mode Fibers Fundamentals*, Springer-Verlag, Germany, 126 (1988).
24. A. Argyros, "Microstructured polymer optical fibers," J. Lightwave Technol. **27**, 1571-1579 (2009).